ACS OMEGA

Open Access
This article is licensed under CC-BY-NC-ND 4.0

http://pubs.acs.org/journal/acsodf
Article

Snap-on Adaptor for Microtiter Plates to Enable Continuous-Flow Microfluidic Screening and Harvesting of Crystalline Materials

Paria Coliaie, Rajan R. Bhawnani, Rabia Ali, Manish S. Kelkar, Akshay Korde, Marianne Langston, Chengxiang Liu, Neda Nazemifard, Daniel B. Patience, Tamar Rosenbaum, Dimitri Skliar, Nandkishor K. Nere, and Meenesh R. Singh*

Cite This: *ACS Omega* 2023, 8, 41502−41511

Read Online

ACCESS | Metrics & More | Article Recommendations | Supporting Information

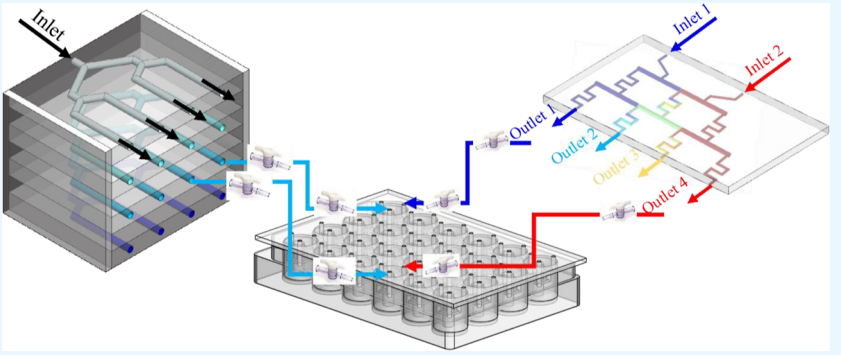

ABSTRACT: Microtiter plate assay is a conventional and standard tool for high-throughput (HT) screening that allows the synthesis, harvesting, and analysis of crystals. The microtiter plate screening assays require a small amount of solute in each experiment, which is adequate for a solid-state crystal analysis such as X-ray diffraction (XRD) or Raman spectroscopy. Despite the advantages of these high-throughput assays, their batch operational nature results in a continuous decrease in supersaturation due to crystal nucleation and growth. Continuous-flow microfluidic mixer devices have evolved as an alternate technique for efficiently screening crystals under controlled supersaturation. However, such a microfluidic device requires a minimum of two inlets per micromixer to create cyclonic flow, thereby creating physical limitations for implementing such a device for HT screening. Additionally, the monolithic design of these microfluidic devices makes it challenging to harvest crystals for post-screening analysis. Here, we develop a snap-on adapter that can be reversibly attached to a microtiter plate and convert it into a continuous-flow microfluidic mixer device. The integration of the snap-on adapter with a flow distributor and concentration gradient generator provides greater control over screening conditions while minimizing the number of independent inlets and pumps required. The three-dimensional (3D)-printed snap-on adaptor is plugged into a 24-well plate assay to demonstrate salt screening of naproxen crystals. Different naproxen salts are crystallized using four different salt formers (SFs)—sodium hydroxide, potassium hydroxide, pyridine, and arginine—and four different solvents−ethanol, methanol, isopropyl alcohol, and deionized water. The wells are further inspected under an optical microscope to identify their morphological forms and yields. The crystals are then harvested for solid-state characterization using XRD and Fourier transform infrared spectroscopy, followed by measurement of their dissolution rates. The flexibility of the snap-on adapter to fit on a wide range of microtiter plates and the ease in harvesting and analyzing crystals postscreening are two significant advantages that make this device versatile for various applications.

1. INTRODUCTION

High-throughput (HT) crystallization screening technologies are vital to the discovery and development of pharmaceuticals as they help in capturing the diversity of solid forms in the early phases of drug development. The discovery and design of solid forms depend on the type of molecule, its physical properties, and the challenges associated with the development processes. In general, the preferred solid form of a compound is the one with the highest thermodynamic stability. The stable form of the parent compound may demonstrate poor solubility or a dissolution rate. Therefore, it is common to prepare salt forms of pharmaceutically acceptable acids and bases to improve the bioavailability of active pharmaceutical ingredients (APIs).[1−4] Depending on the intended target property, there can be a wide

Received: July 27, 2023
Accepted: October 5, 2023
Published: October 23, 2023

ACS Publications
© 2023 The Authors. Published by American Chemical Society

https://doi.org/10.1021/acsomega.3c05478
ACS Omega 2023, 8, 41502−41511

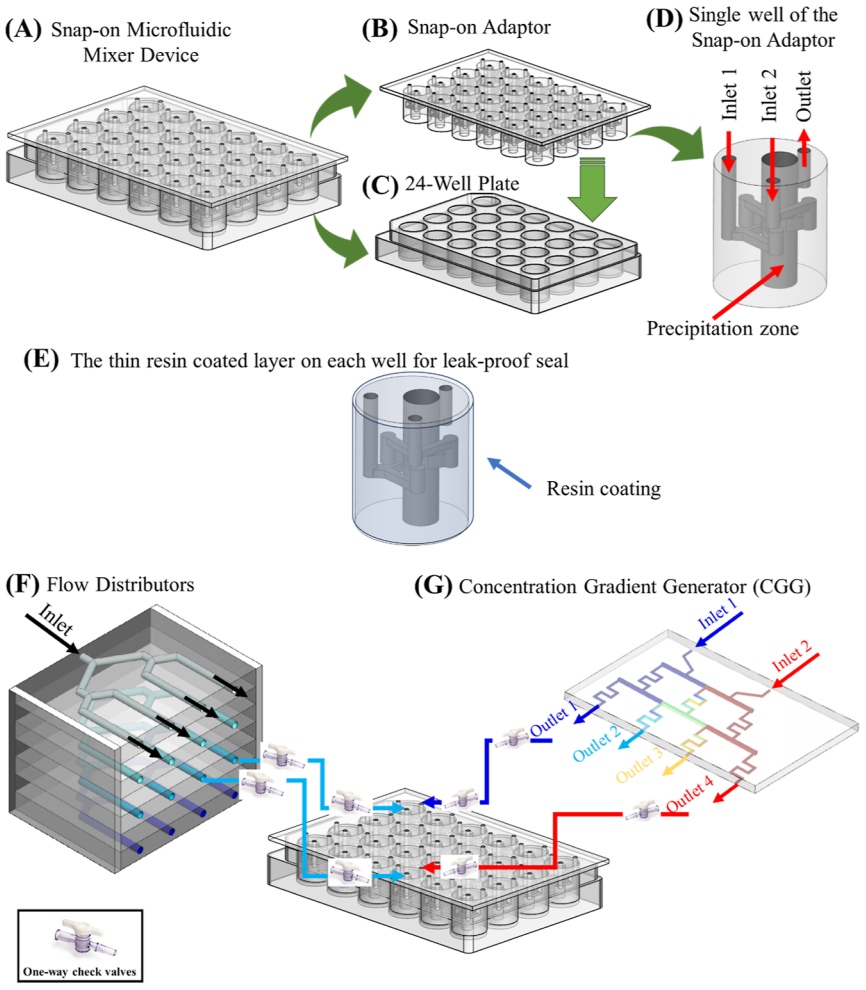

Figure 1. 3D design of an (A) 24-well plate snap-on microfluidic mixer device, (B) snap-on adaptor, and (C) 24-well plate assay; (D) enlarged view of a single well of the snap-on adaptor; (E) thin coat of resin applied on the outer cylinders and cured to ensure the leak-proof seal; (F) four sets of flow distributor in a stack, and (G) CGG connected to the snap-on adapter.

range of polymorphic, solvated, or hydrated forms of pharmaceutical salts. The physicochemical properties of different salts, such as solubility, morphology, density, and the physical and chemical stability of a single organic cation, can differ significantly. The HT solid form screening aims to determine the desired crystal form as a preventative measure against unwanted outcomes later in process development.

HT screening devices based on wells or vials are usually used to analyze the crystal structure of newly synthesized compounds and to discover possible new crystal forms. Microtiter plate assays are available with volumes ranging from 1 mL to 1L and can assess up to 10,000 conditions per day.[5] Furthermore, the apparatuses for HT screening can be fully automated and allow for solid-state studies of crystals by either X-ray diffraction (XRD) or Raman spectroscopy.[6,7]

With the advances of miniaturized systems, screening techniques have evolved to accommodate multiple experiments in a single device. Currently examined screening techniques resemble well-mixed batch crystallizers. While the temperature and solvent composition can be maintained constant and controlled in batch systems, the concentrations can vary. The crystal nucleation and growth in batch systems cause a decrease in solute concentration and thereby supersaturation, which is a driver for crystallization. Hence, the polymorphs, morphology, crystallization kinetics, and crystal size discovered during initial screening may not remain constant. Attempts have been made to facilitate continuous-flow screening by designing a complementary part for existing HT batch systems. Murphy and co-workers previously developed a continuous-flow HT screening by designing a passive microassembly of a fluidic control.[8] Continuous flow polymerase chain reaction chips (FPCRs) were combined with 12 networks that distributed the same polymerase chain reaction (PCR) cocktail to eight different devices in each column. A double-sided hot embossing technique was used to fabricate the fluid-control and multiwell (MW) CFPCR chips. This combination utilizes the existing advantages of MicroCFPCR devices, including rapid reactions and reduced reagent consumption, in continuous flow mode. In another study, Murphy and co-workers designed, configured, and fabricated continuous flow thermal arrays of reactors in a 96-device.[9] The dimensions for the nanoliter CFPCR were chosen using finite element analysis based on a series of thermo-fluidic models. With these HT-96 CFPCR devices, DNA samples could be amplified rapidly, providing the results at the right time. The advancement of 3D printing has enabled the direct printing of microfluidic devices. However, it is limited to oxygen-impermeable materials. Eddington et al. studied 3D-printed microfluidic devices with gas-permeable PDMS membranes for an oxygen-control cell culture assay.[10] A 3D-printed device coupled with gas-permeable membranes was applied to a 24-well

https://doi.org/10.1021/acsomega.3c05478
ACS Omega 2023, 8, 41502−41511

oxygen control device for standard MW plates. Using this device, they controlled four different oxygen levels and maintained six wells at each oxygen level. In the studies presented here, the capability of adding a control layer to existing HT systems proved to be beneficial.

Novel continuous-flow microfluidic devices are implemented to avoid the issues of a conventional batch system by controlling supersaturation.[11] The novel systems allow for the evaluation of crystal polymorphs and their morphology at controlled supersaturation. Microfluidic devices that utilize a continuous-flow mode of operations and enable controlled conditions are proven effective for determining the crystal polymorph, morphology, size, and kinetics.[9,12−14] This microfluidic mixer device creates cyclonic flow, ensuring uniform mixing and constant supersaturation inside the mixer.[15] This well-mixed continuous-flow microfluidic device technology was advanced for enabling the parallel screening of crystalline materials under controlled conditions.[16] Even though MW microfluidic technology offers many advantages, the device still poses difficulties for HT screening (such as salt screening) that demands multiple flow handling equipment.

This study aims to develop a snap-on adaptor that can transform any microtiter plate assay into a continuous-flow microfluidic mixer with a minimum requirement for fluid handling systems. The snap-on adapter includes the design of the cyclone mixer, with the merged inlet design where each inlet enters into the cyclone mixer from two channels, providing homogeneous mixing for every well.[17] The inlets of the snap-on adapter can be connected to the flow distributor or concentration gradient generator (CGG).[18,19] By offering different combinations of the flow distributor and the CGG, the experimental design becomes more flexible. Moreover, the technology of 3D printing has considerably eased the fabrication process of multilayer snap-on adaptors compared to conventional microfabrication techniques.

Here, a 24-well plate was converted into a snap-on microfluidic device that was evaluated for the screening of naproxen salt. Different types of naproxen salt forms were identified and characterized more rapidly and comprehensively by using this HT technology. This study screened naproxen salts of sodium hydroxide, potassium hydroxide, pyridine, and arginine using different solvents listed as ethanol, methanol, isopropyl alcohol (IPA), and deionized (DI) water. The snap-on microfluidic device also provides a means to harvest newly formed crystals after screening for further analysis. The harvested crystals can be characterized using optical microscopy, XRD, and Fourier transform infrared spectroscopy (FT-IR).

2. THEORETICAL METHODS

2.1. Flow Distribution Strategies for Snap-on Adaptor Design. The 24-well plate assay was converted to a continuous-flow microfluidic mixer device using a snap-on adapter. The assembly of the 24-well plate with the snap-on microfluidic mixer includes two compartments that are connected using tubes, fittings, and one-way check valves. The first part is the snap-on adaptor inserted inside a 24-well plate assay (see Figure 1A). The detailed measurements of this part are provided in Section S1 of the Supporting Information. The second compartment of this system is a network of microchannels that distribute solutions into wells. Each well in the snap-on adaptor part had an identical configuration to the merged inlet microfluidic device, which was previously developed.[16] The overall size of a single well and the merged connections were equal to the inner diameter of a single well in a 24-well plate assay. Similar to the merged inlet design, each well had two major inlets indicated with red arrows in Figure 1D. The major inlets of each well were then connected to an array of microchannels responsible for distributing the solutions inside the microfluidic mixer device. Here, two commonly used flow distribution designs were used to distribute the solutions into the snap-on adaptor microfluidic mixer device. The first design is the flow distributor design that equally distributes the entering stream to four channels (see Figure 1E).[20,21] The flow distributor design was used to connect a 4 × 4 subarray of wells, as shown in Figure 1E. These 16 wells were operated in a continuous-flow manner using only eight syringe pumps. The eight different solutions entering into these arrays resulted in 16 different conditions. The remaining eight wells (the 2 × 4 subarray) were operated using the flow distributor and CGG. The design of the CGG is shown in Figure 1F. In the CGG, two different solutions were premixed to generate four different concentrations, each sent into different channels.[19,22] The dimensions of the snap-on adaptor, flow distributor, and CGG are provided in Section S1 of the Supporting Information.

2.2. Computational Fluid Dynamics Simulation to Obtain Velocity and Concentration Profiles. The design of each well in the snap-on adaptor was similar to the design of the previously developed merged-inlet micromixers.[16] The effectiveness of mixing for each well was evaluated by calculating the velocity, pressure, and concentration profiles in the snap-on microfluidic mixer device. The CAD file for design for the inner channels and wells was imported in COMSOL Multiphysics and meshed using a free tetrahedral mesh of element size 0.00789−0.00142 mm and a curvature factor of 0.6. The maximum element growth rate and the resolution of the narrow region were kept at 1.5 and 0.5, accordingly. The Navier−Stokes equation coupled with the continuity equation was solved to mix pure streams of API in the solvent (naproxen in ethanol) and salt former (SF) solution (NaOH in ethanol). The boundary conditions on inlets were set according to the entering flow rates of the API and SFs. In addition, the boundary condition at the outlet was set to zero diffusive flux for the continuity equation and fixed ambient pressure for the Navier−Stokes equation. The concentration-dependent viscosity and density of the water/ethanol mixture were considered in the model. Details of the selected boundary conditions and model parameters are provided in Section S2 of the Supporting Information. The algebraic multigrid solver (GMRES solver) was used as a linear solver with a residual tolerance of 0.01. A maximum number of iterations of 200 was used to calculate the velocity profile in each well for a 16-well device operated with only eight inlets. The calculated velocity profile was then coupled with mass balance equations to calculate the concentration profile in the snap-on microfluidic mixer device. The coupled system of equations was solved using direct as the linear solver (MUMPS) and the Newtonian nonlinear method with a relative tolerance of 0.001.

3. MATERIALS AND EXPERIMENTAL METHOD

3.1. Materials. The crystalline naproxen (Sigma-Aldrich, chemical purity ≥98%) was used for the HT continuous-flow salt screening. The selected SFs for this study were sodium hydroxide (Sigma-Aldrich), potassium hydroxide, pyridine, and L-arginine. All solvents used for salt screening were purchased from Sigma-Aldrich with the following purities: DI water (Sigma-Aldrich, 18 MΩ cm), ethanol, methanol, and 2-propanol (IPA).

https://doi.org/10.1021/acsomega.3c05478
ACS Omega 2023, 8, 41502−41511

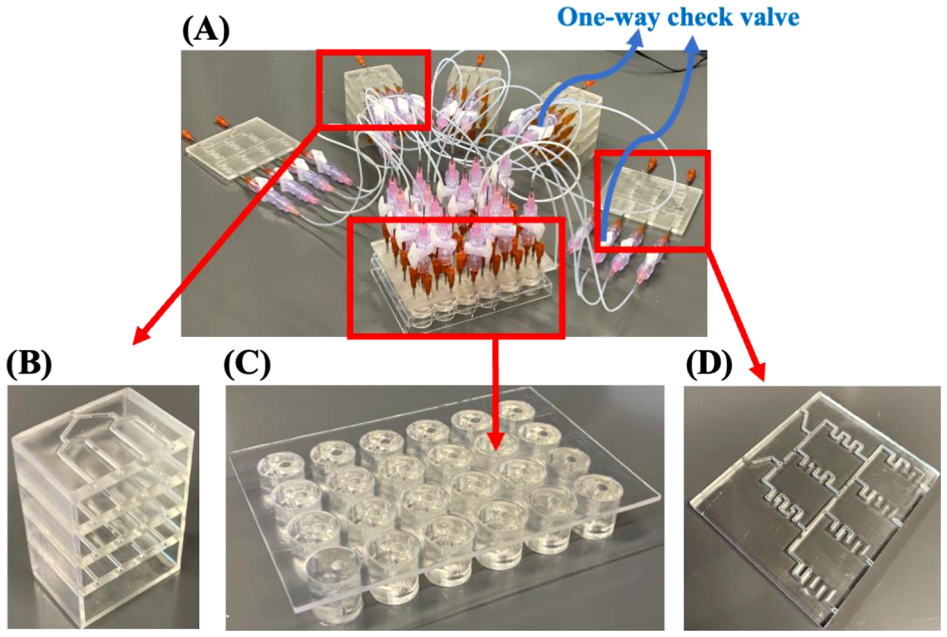

Figure 2. (A) Experimental setup for the snap-on microfluidic mixer device connecting flow distributor and CGG to the snap-on adapter; (B) four sets of flow distributor arrays; (C) snap-on adaptor showing snap-on adapter plugged into the 24-well plate assay; (D) CGG;

3.2. Fabrication of the Snap-on Microfluidic Mixer Device. The 3D design of the snap-on adaptor for a 24-well plate assay shown in Figure 1A was designed in SolidWorks (2020, Dassault Systems). A stereolithography (SLA) 3D printer (form 3, Formlabs Inc., USA) was used to print all parts. A clear FLGPCL02 resin activated by a 405 nm laser was used to 3D print optically clear microfluidic devices with 150 μm of lateral and 25 μm of axial resolutions. The 3D-printed parts were washed with an IPA (90%, Sigma-Aldrich) bath for 60 min in the Form Wash (Formlabs Inc., USA) to remove the residues of the resin from the external surface. The generated support structures of the 3D-printed parts were loosened after the washing procedure, and their removal did not require much effort. All the interior channels of the 3D-printed device were washed separately by injecting IPA using a syringe, followed by passing air from inlets to ensure complete removal of the uncured resins from all of the channels. The careful selection of the layouts for prints on the 3D printer stage minimized the contact of the supports with the top and bottom surfaces. However, if necessary, the optical transparency could be improved by wet sanding using 400 to 12,000 grit pads, followed by spray painting of resin. The bottom side of the snap-on adaptor part was kept open (see Figure 1B) because it was sealed when inserted into the 24-well plate assay. The outer walls of each cylinder in the snap-on part were covered with a thin layer of resin (Figure 1D). After plugging in the snap-on adaptor, the snap-on microfluidic device was cured and to ensure a leak-proof seal. The top part of the snap-on adaptor was sealed separately by applying a thin layer of the resin around each opening and then putting small polycarbonate film. The top part was cured for around 10 min to seal all of the openings. The fabricated snap-on adaptor is shown in Figure 2. Details of the fabrication procedure of the snap-on adaptor, flow distributor, and CGG are provided in Section S1 of the Supporting Information.

3.3. Experimental Setup. Figure 2 shows the experimental setup for the salt screening of the naproxen using a 24-well plate assay coupled with the snap-on adaptor, flow distributor, and CGG. As shown in Figure 2A, the snap-on part was inserted into a 24-well plate assay, and then inlet connections on top were connected to output channels of the flow network externally. The separation of the connections from the snap-on part helps eliminate the possible disturbances to the system that might result in the pressure difference from the pump inlets to the outlets of each well. In addition, it allows for implementing the microfluidic one-way check valves before the major inlets of each well. Implementation of the one-way check valves guaranteed the equal distribution of flow into the outlet streams. The 24-plate assay was divided into two subarrays where different flow networks were used. The first subarray included 16 wells (a 4×4 subarray), where every four wells on a single row or column were connected using one inlet. Thus, eight flow distributor arrays were required for screening 16 different conditions in the first subarray.

Among these eight streams, four were naproxen solutions in different solvents: ethanol, methanol, IPA, and DI water. The other four inlets were ethanoic solutions of the different SFs: sodium hydroxide, potassium hydroxide, pyridine, and arginine. Comparing to the previously developed merged inlet microfluidic mixer design, the 4×4 subarray of the snap-on microfluidic mixer device required one-fourth of the required pumps. The remaining eight wells of the microtiter plate were divided into two sets of the 4×1 subarrays. A flow distributor and CGG were used in each 1×4 subarray to screen concentration gradients of either the API or SF. For every 1×4 subarray, three pumps were required since each CGG required two inflows at different concentrations and each flow distributor needed one inflow. As shown in Figure 2, one-way check valves were installed at the outlet of the flow distributor, CGG, and the inlet of the snap-on adaptor. The snap-on adaptor was connected to the flow distributor and CGG by using equal-length tubing for all inlets. Every single outlet stream was also collected separately for further analysis.

3.4. Characterization. Optical images of the naproxen salts were taken using an optical microscope (Olympus BX53M, Olympus America Inc.). The in situ FT-IR measurements were done using an INVENIO S FT-IR spectrometer coupled with a

https://doi.org/10.1021/acsomega.3c05478
ACS Omega 2023, 8, 41502−41511

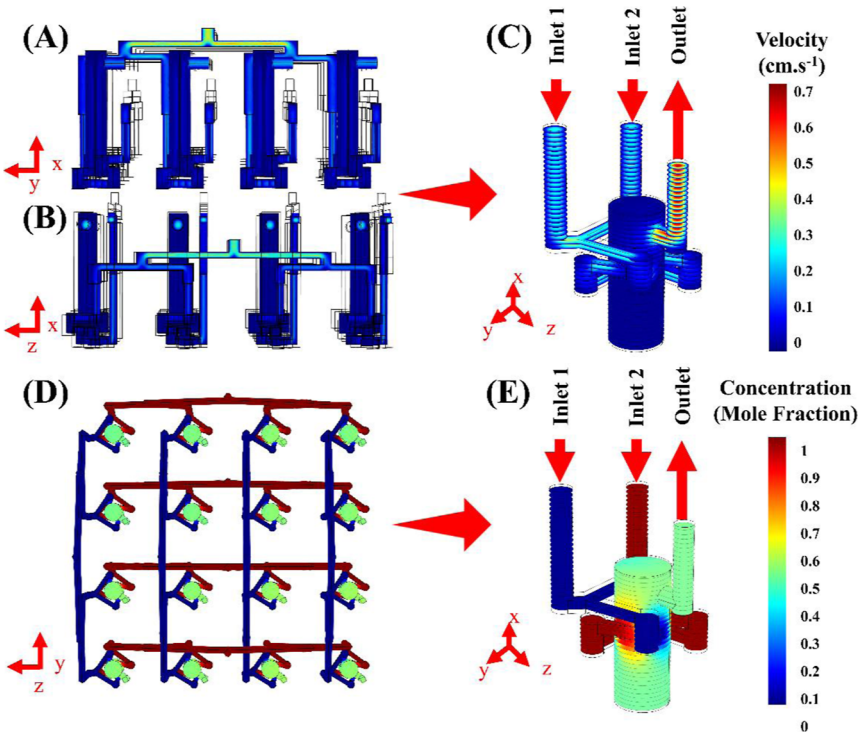

Figure 3. Steady-state velocity profile of a 4 × 4 subarray of the 24-well plate snap-on microfluidic mixer device of (A) inlet 1, and (B) inlet 2; (C) steady-state velocity profile of a single well in the 4 × 4 subarray; steady-state concentration profile of (D) a 4 × 4 subarray of the 24-well plate snap-on microfluidic mixer device; (E) a single well in the 4 × 4 subarray.

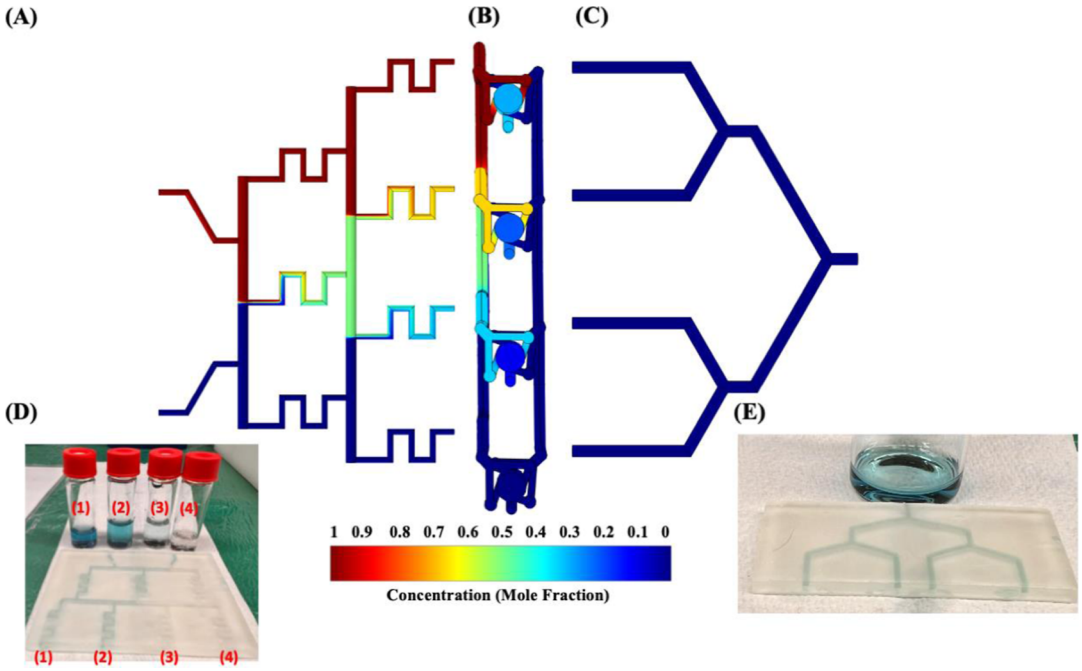

Figure 4. Steady-state concentration profile in the (A) CGG, (B) 4 × 1 subarray of the 24-well plate snap-on microfluidic mixer device, (C) flow distributor, and (D) dye experiment conducted with CGG by feeding a blue-colored dye solution and water. The concentrations obtained in vials (1), (2), (3), and (4) are 100, 75, 25, and 0% of the dye solution fed to CGG, (E) the same dye solution was fed to the flow distributor at 1 mL/min flow rates. The flow rates measured from four outlets were similar and close to 0.25 mL/min.

Pike demountable transmission flow cell. The XRD measurements were performed on a Scintag XDS 2000 diffractometer with Cu Kα radiation.

The kinetics of the dissolution rate measurement of the naproxen salts was investigated using electrochemical impedance spectroscopy (EIS) of the naproxen salts in water.[23] A three-electrode cell with Ag/AgCl as the reference electrode and Pt plates as the counter and the working electrode was used to measure the solution resistance. The cell was initially filled with DI water, and then a known amount of each salt was added to it.

https://doi.org/10.1021/acsomega.3c05478
ACS Omega 2023, 8, 41502−41511

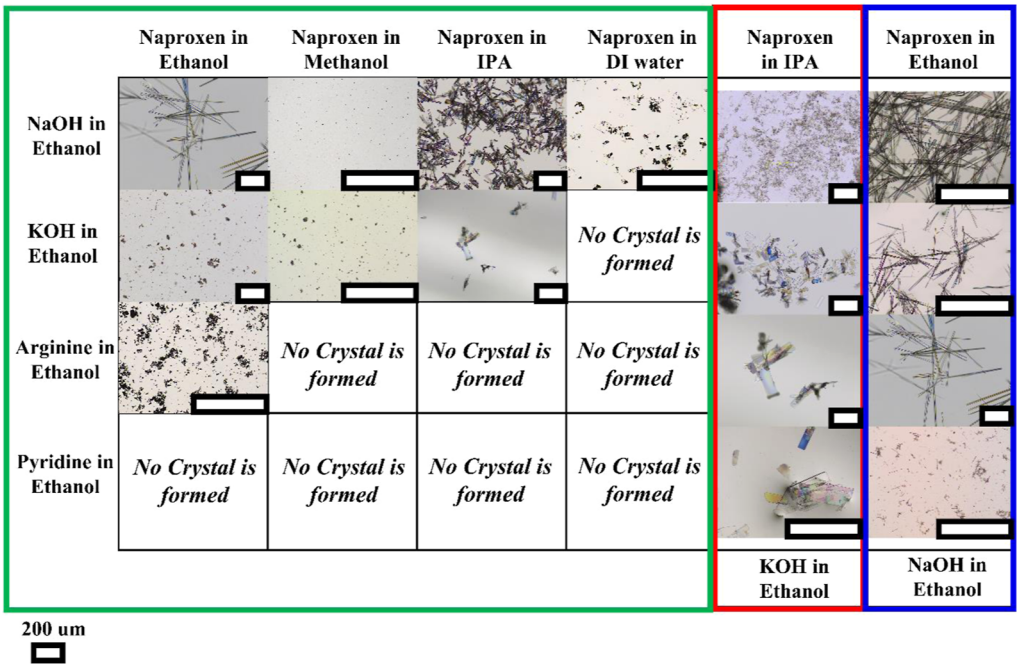

Figure 5. Optical images of naproxen salt screening in a snap-on microfluidic mixer device. The green box shows the 4 × 4 subarray, where one flow distributor was used for each column and row. The red and blue boxes each show a 4 × 1 subarray where a combination of flow distributor and CGG were used to distribute the solutions in the wells. The wells where no crystal was formed are labeled as "No crystal is formed".

The change in the solution resistance was measured vs time and calibrated for the amount of dissolved salts. The details for the calculation and measurements are provided in Section S2 of the Supporting Information.

4. RESULTS AND DISCUSSION

4.1. Velocity and Concentration Profiles. The velocity profile is calculated in the microfluidic device to evaluate the pressure drop across all wells in the microfluidic system. The calculation of the velocity and pressure profiles involves solving the incompressible Navier−Stokes equation in the microfluidic channels. The objective is to design the snap-on adapter for a uniform pressure drop across all wells in the microfluidic system. Since these wells are connected with a common feed that splits and recombines to attain different compositions inside the well, it is important to ensure that there will not be unequal flow distribution among the wells. Only after such calculations can we 3D-print the device and validate the expected composition variation across the wells. The steady-state velocity and concentration profiles in the snap-on adapter are shown in Figure 3. The velocity profile of the 4 × 4 subarray is shown in Figure 3A,B. Since it is necessary to obtain an equivalent level of mixing efficiency in each well, the goal here is to evaluate the velocity profile in all 16 wells when identical boundary conditions were applied at the main inlets for the API and SF solutions. Figure 3A,B shows that applying these boundary conditions resulted in a similar velocity profile in the 16 wells, confirming that there is no backflow. To better understand the velocity profile inside each well, the velocity profile inside one of the wells is shown in Figure 3C. The two streams of API solution and SF solution entered from inlets 1 and 2 on the top are mixed in the cylindrical zone. The outlet connection was provided above both inlets. Using these velocity profiles, the concentration profile in the 4 × 4 array was calculated and shown in Figure 3D. Identical concentration profiles in all 16 wells confirmed the identical mixing efficiencies across all the wells of the snap-on microfluidic mixer device. Figure 3E shows an enlarged view of the concentration profile of a single well for clarity.

The concentration profile of the 4 × 1 subarray is shown in Figure 4B. This subarray required a combination of flow distributor and CGG. In Figure 4A, the concentration profile in the CGG is shown. Two streams with initial mole fractions of 0 and 1 were pumped in to generate four streams of concentrations of 0, 0.25, 0.75, and 1. In Figure 4C, the concentration profile of a flow distributor is shown. Connecting the flow distributor and CGG to the 4 × 1 subarray resulted in the concentration profile shown in Figure 4B.

4.2. Experimental Results. *4.2.1. Optical Characterization of Naproxen Salts.* The optical images of the naproxen salts formed in the 24-well plate snap-on microfluidic mixer device are shown in Figure 5. The results from the 4 × 4 subarray are enclosed in the green square. The prepared naproxen solutions (in ethanol, methanol, IPA, and DI water) were distributed into the columns of the 4 × 4 subarray. The SF solutions were also fed into the 4 × 4 subarray using the flow distributor arrays. One flow distributor array was used to distribute the SF solutions into wells in each row. The continuous-flow screening of these 16 conditions resulted in the formation of salts in 50% of the wells after 30 min of screening. The most formed salt was sodium naproxen (see the wells in the first row). Sodium hydroxide dissolved in ethanol reacted with all naproxen solutions (ethanol, methanol, IPA, and DI water) and formed naproxen sodium salt.

The crystals formed with naproxen solution in ethanol had a needle-shaped morphology and a high aspect ratio. The sodium naproxen salt from the naproxen solution in IPA had more like a plate-shaped morphology and a lower aspect ratio than the previously discussed salts. The formation of naproxen salt from the naproxen solution in methanol resulted in very tiny crystals, and the morphology could not be reported using optical images.

https://doi.org/10.1021/acsomega.3c05478
ACS Omega 2023, 8, 41502−41511

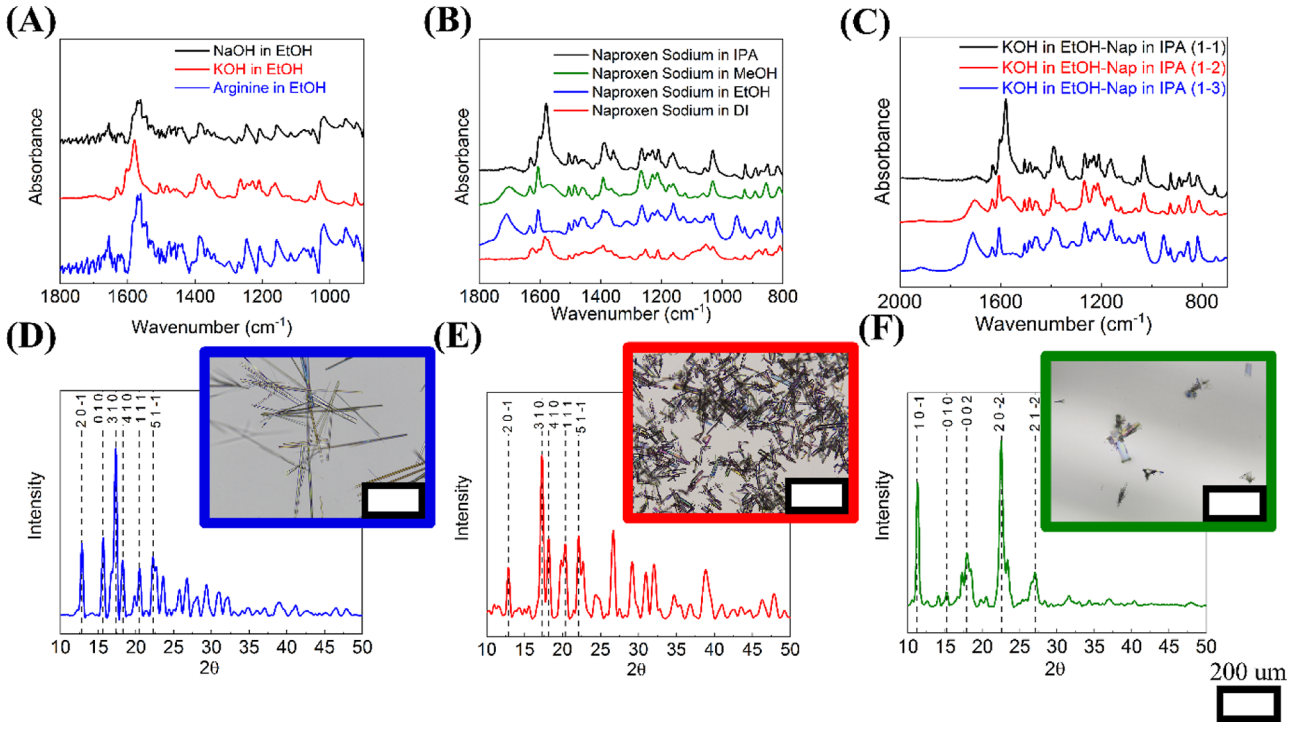

Figure 6. (A) FT-IR spectra of sodium, potassium, and arginine naproxen salts (B) FT-IR spectra of the naproxen sodium salts formed with sodium hydroxide in ethanol and naproxen in different solvents as listed: IPA, methanol, ethanol, and DI water; (C) FT-IR spectra of naproxen salts formed from potassium hydroxide in ethanol as a SF and naproxen in IPA; XRD pattern of naproxen salts: (D) naproxen sodium formed from naproxen in ethanol and NaOH in ethanol; (E) sodium naproxen formed from naproxen in IPA and NaOH in ethanol; and (F) naproxen potassium formed from naproxen in IPA and KOH in ethanol.

The majority of the formed salts from an aqueous solution of naproxen had a plate-shaped morphology but were not uniform in size.

The potassium solution salted out naproxen potassium in 75% of the wells. The formation of potassium naproxen salts with the naproxen solutions in ethanol and methanol resulted in tiny crystals similar to those of sodium naproxen salts formed from the methanol solution of naproxen and sodium hydroxide. The morphology of these tiny crystals was not fully detected using the optical images, and the quantity of these formed salts was not enough for XRD. The naproxen solution in IPA formed plate-shaped crystals when mixed with sodium hydroxide and potassium hydroxide. The combination of naproxen in IPA and arginine or pyridine did not form any naproxen salts. The aqueous solution of naproxen only salted out under 25% of the conditions. As shown in Figure 5, a mixture of 2D, plate-shaped crystals, and agglomerated particles was formed where an aqueous solution of naproxen was mixed with sodium hydroxide. The arginine naproxen salt only formed when a naproxen solution in ethanol was used, resulting in small naproxen salts. Comparing the SFs according to the number of salts formed, the order was NaOH > KOH > L-arginine > pyridine. Arginine did not salt out naproxen in 75% of the wells, and pyridine was the only SF solution that did not salt out with naproxen in any conditions.

The red and blue boxes in Figure 5 show the optical images of the naproxen salts formed in two 4 × 1 subarrays of a 24-well plate. An ethanolic solution of potassium hydroxide was distributed into the four wells by using a flow distributor for the wells shown in the red box. For the second inlet, two different concentrations of the naproxen solution in IPA were mixed and distributed into these four wells using a CGG. As a result, the concentration of the SF was constant in all these four wells, while the concentration of naproxen solution in IPA was varied. As shown in Figure 5, potassium naproxen salt was formed in all four wells shown in the red box. As the concentration of naproxen increased, the yield and aspect ratio of the plate-shaped salt crystals increased. The second 4 × 1 subarray shown within the blue box had the same configuration for the solution distribution. The ethanolic sodium hydroxide solution was distributed into all four wells on the sixth column using a flow distributor. For the second inlet, two different concentrations of the ethanolic solution of naproxen were mixed in a CGG to distribute four different concentrations of the naproxen salts into the wells. The sodium naproxen salts formed in these wells had a needle-shaped morphology. The formation yield and aspect ratio of the crystals increased with the increase in the naproxen concentration.

4.2.2. Qualitative Screening of Naproxen Salts Using FT-IR. FT-IR analysis was performed to characterize the naproxen salts formed in the snap-on continuous-flow microfluidic mixer device. Figure 6A shows the FT-IR spectra of the three different crystallized naproxen salts: sodium naproxen, potassium naproxen, and arginine naproxen. These salts were formed from an ethanolic solution of naproxen and different SF solutions. While different naproxen salts were expected to show different spectra, naproxen sodium salts from different solutions show identical FT-IR spectra. Figure 6B shows the naproxen sodium salts formed from the reaction between an ethanolic solution of sodium hydroxide and naproxen in four different solvents listed as ethanol, methanol, IPA, and DI water. All four spectra show identical peaks, confirming the formation of naproxen sodium salts from these four wells.

https://doi.org/10.1021/acsomega.3c05478
ACS Omega 2023, 8, 41502−41511

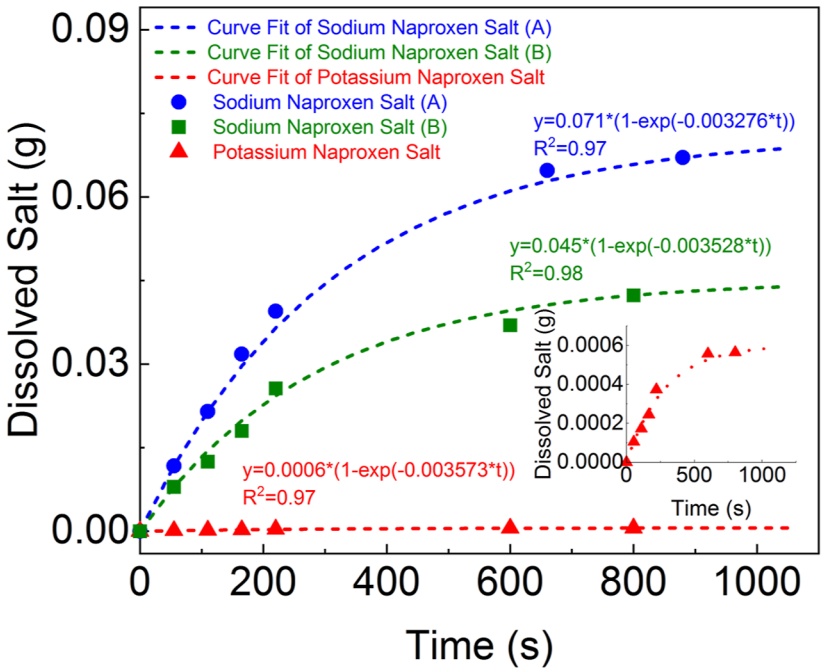

Figure 7. Dissolution rate comparison of naproxen salts: the fitted line for the blue circles shows the dissolution rate of sodium naproxen salt that was formed from an ethanolic solution of naproxen; the fitted line for the green squares shows the dissolution rate of sodium naproxen salt that was formed from naproxen in IPA; the fitted line for the red triangles shows the dissolution rate of potassium naproxen. [The smaller inset graph (red curve) shows a larger view of the curve fit for the potassium naproxen salt].

Another FT-IR analysis was performed by studying the spectra of the potassium naproxen salts formed at different ratios of the naproxen and SF solution. Figure 6C shows that the four crystallized potassium naproxen salts have identical characterization peaks in their FT-IR spectra.

4.2.3. Dissolution Rate Measurements and XRD Analysis of Naproxen Salts. Among all of the formed naproxen salts, only three of them had a high enough yield to salt out naproxen in a reasonable quantity. The rest of the wells had less naproxen salt formed inside, which was impossible to filter and dry for further analysis. From here, the sodium naproxen salt formed in naproxen solutions in ethanol and IPA and the potassium naproxen salt formed in IPA were filtered and dried for XRD and crystal structure analysis and measurement of the dissolution rate. The XRD pattern of the salts with the highest yields is shown in Figure 6D−F.[24] The needle-shaped crystals of naproxen sodium from ethanol and IPA solutions showed similar XRD patterns. However, potassium naproxen with the plate-shaped morphology showed a different XRD pattern in Figure 6F. The details of the calculation of Miller indices and lattice parameters are provided in Section S4.3 of the Supporting Information.

The dissolution rate of the three salts mentioned above was calculated using EIS. The change in the resistance of the pure water vs time was measured for a known amount of added naproxen salt using a three-electrode cell. In Figure 7, the dissolved amount of salt vs the time is shown for all three salts. The slopes of the fitted lines are reported as the dissolution rate and are shown in Figure 7. The results showed that the sodium naproxen salts had significantly higher solubility compared to the potassium naproxen salt.

5. CONCLUSIONS

The effective and robust screening of possible crystal forms of newly synthesized drugs requires modification of existing batch HT screening techniques to maintain stable solution conditions. The batch HT technologies involving microtiter assay suffer from depletion of the supersaturation inside the microwells due to crystal nucleation and growth. The screening results obtained under such varying solution conditions are often misleading. This study develops a novel snap-on adaptor that converts a batch microtiter plate into a continuous-flow microfluidic mixer device. The continuous-flow HT technique enables the effective and robust screening of crystal polymorph, morphology, size, and kinetics under controlled conditions. Here, the design of the snap-on adaptor is based on the previously developed continuous-flow microfluidic mixer that creates cyclonic flow in each well for efficient mixing and captures crystals that can be easily harvested for characterization and further evaluation.

Here, a snap-on adaptor is developed for a 24-well plate to enable continuous-flow salt screening of naproxen. The continuous-flow operation of the snap-on microfluidic mixer device requires implementing flow distribution networks to distribute solutions into all wells while minimizing the number of pumps. Two types of flow distribution networks are introduced in this study to expand the capabilities of continuous-flow HT screening. The first one is the flow distributor that can equally distribute a single entering stream into multiple channels (e.g., two, four, eight, 16, etc.). The second type of flow network is a CGG. The CGG requires two entering streams of different concentrations that are split and mixed to obtain a range of concentrations that can be fed to the snap-on adapter. Different combinations of these two types of distribution flow networks allow for different screening experiment designs.

In this study, a 24-well plate assay is divided into two subarrays. The first one is a 4 × 4 subarray of wells, and multiple flow distributors are implemented to screen 16 different conditions. First, naproxen is dissolved in four different solvents, listed as ethanol, methanol, IPA, and DI water, and each is

https://doi.org/10.1021/acsomega.3c05478
ACS Omega 2023, 8, 41502−41511

distributed into four wells with a flow distributor. Then four different SFs listed as sodium hydroxide, potassium hydroxide, arginine, and pyridine are dissolved in ethanol and distributed into the wells using flow distributors. On the remaining part of the 24-well plate assay, a combination of flow distributor and CGG is used for every four wells to screen for different SFs and naproxen solution ratios. After continuous-flow screening, optical images are taken from the crystallized salts in the wells. Naproxen is salted out in 50 percent of the conditions; however, not all salts have a high formation yield. Therefore, FT-IR analyses are performed on the crystallized salts of naproxen to identify the formation of different salts. Among the crystallized salts, three have high formation yields, where the quantity is enough for comparison. These three salts are filtered and dried for XRD analysis and dissolution rate measurements. The dissolution rate of these salts is measured using the EIS technique. Resistance of the solution is measured over time as a function of salt concentration and correlated to calculate the dissolution rate. The results show that the naproxen sodium salt has around 2 orders of magnitude higher dissolution rate than the potassium naproxen salt.

The flexibility of snap-on adapters to fit different types of microtiter plates, in combination with different types of flow distributors, provides opportunities to use the snap-on microfluidic device for a range of HT screening applications. These efficient HT screening techniques will have a transformative impact on material discovery and development for various healthcare and energy applications.

■ ASSOCIATED CONTENT

Supporting Information

The Supporting Information is available free of charge at https://pubs.acs.org/doi/10.1021/acsomega.3c05478.

Designs and dimensions of a snap-on microfluidic device; COMSOL simulation details; fabrication details for 24-well snap-on adapter; additional experimental details including operating conditions for salt screening of Naproxen, dissolution rate measurements, lattice structure of Naproxen crystals, and screening results in batch and flow modes of operation; and circuit diagram showing fluidic connection between flow distributor, CGG, and snap-on adapter (PDF)

■ AUTHOR INFORMATION

Corresponding Author

Meenesh R. Singh − *Department of Chemical Engineering, University of Illinois at Chicago, Chicago, Illinois 60607, United States;* orcid.org/0000-0002-3638-8866; Phone: (312)413-7673; Email: mrsingh@uic.edu

Authors

Paria Coliaie − *Department of Chemical Engineering, University of Illinois at Chicago, Chicago, Illinois 60607, United States;* orcid.org/0000-0002-9603-6168

Rajan R. Bhawnani − *Department of Chemical Engineering, University of Illinois at Chicago, Chicago, Illinois 60607, United States*

Rabia Ali − *Department of Chemical Engineering, University of Illinois at Chicago, Chicago, Illinois 60607, United States*

Manish S. Kelkar − *Center of Excellence for Isolation & Separation Technologies (CoExIST), Process R&D, AbbVie Inc., North Chicago, Illinois 60064, United States*

Akshay Korde − *Center of Excellence for Isolation & Separation Technologies (CoExIST), Process R&D, AbbVie Inc., North Chicago, Illinois 60064, United States;* orcid.org/0000-0003-3811-5172

Marianne Langston − *Pharmaceutics Research—Analytical Development, Takeda Pharmaceuticals International Co., Cambridge, Massachusetts 02139, United States*

Chengxiang Liu − *Pharmaceutical Development, Biogen, Cambridge, Massachusetts 02142, United States*

Neda Nazemifard − *Pharmaceutics Research—Analytical Development, Takeda Pharmaceuticals International Co., Cambridge, Massachusetts 02139, United States;* orcid.org/0000-0001-9575-5243

Daniel B. Patience − *Chemical Process Development, Biogen, Cambridge, Massachusetts 02142, United States;* orcid.org/0000-0001-5739-3384

Tamar Rosenbaum − *Bristol-Myers Squibb Co., Drug Product Science & Technology, New Brunswick, New Jersey 08901, United States;* orcid.org/0000-0003-1521-8865

Dimitri Skliar − *Bristol Myers Squibb Co., Chemical & Synthetic Development, New Brunswick, New Jersey 08901, United States*

Nandkishor K. Nere − *Department of Chemical Engineering, University of Illinois at Chicago, Chicago, Illinois 60607, United States; Center of Excellence for Isolation & Separation Technologies (CoExIST), Process R&D, AbbVie Inc., North Chicago, Illinois 60064, United States;* orcid.org/0000-0002-9971-1990

Complete contact information is available at: https://pubs.acs.org/10.1021/acsomega.3c05478

Notes

The authors declare the following competing financial interest(s): A PCT application (PCT/US20/36353) titled Continuous-Flow, Well Mixed, Microfluidic Crystallization Device for Screening Polymorphs, Morphologies and Crystallization Kinetics at Controlled Supersaturation has been filed. Data were generated by the University of Illinois Chicago. AbbVie Inc., North Chicago, USA, provided experimental support for a summer internship of Paria Coliaie. Dr. Manish S. Kelkar, Dr. Akshay Korde, and Dr. Nandkishor K. Nere are present employees of AbbVie Inc.

■ ACKNOWLEDGMENTS

This material is based on the work performed in the Materials and Systems Engineering Laboratory at the University of Illinois Chicago in collaboration with Enabling Technology Consortium (ETC: https://www.etconsortium.org/, specifically AbbVie, Biogen, Bristol Myers Squibb, and Takeda Pharmaceuticals). P.C. and M.R.S. acknowledge funding support from ETC to conduct this work. P.C. acknowledges the summer internship opportunity at AbbVie Inc. to conduct a few experiments for the completion of this work. The authors also thank Moussa Boukerche, Jie Chen, Daniel Pohlman, Bradley Greiner, Pankaj Shah, and Kushal Sinha for their comments and suggestions.

■ REFERENCES

(1) Semin, D. J.; Jona, J.; Peterson, M. L.; Zanon, R. Salt Screening and Selection. *Burger's Medicinal Chemistry and Drug Discovery*; Wiley, 2003; pp 381−400.

(2) Neau, S. H. Pharmaceutical salts. *Water-Insoluble Drug Formulation*; CRC Press, 2008; pp 431−450.

(3) Gupta, D.; Bhatia, D.; Dave, V.; Sutariya, V.; Varghese Gupta, S. Salts of therapeutic agents: chemical, physicochemical, and biological considerations. *Molecules* **2018**, *23*, 1719.
(4) Fernández Casares, A.; Nap, W. M.; Ten Figás, G.; Huizenga, P.; Groot, R.; Hoffmann, M. An evaluation of salt screening methodologies. *J. Pharm. Pharmacol.* **2015**, *67*, 812−822.
(5) Bevan, C. D.; Lloyd, R. S. A high-throughput screening method for the determination of aqueous drug solubility using laser nephelometry in microtiter plates. *Anal. Chem.* **2000**, *72*, 1781−1787.
(6) Trietsch, S. J.; Israëls, G. D.; Joore, J.; Hankemeier, T.; Vulto, P. Microfluidic titer plate for stratified 3D cell culture. *Lab Chip* **2013**, *13*, 3548−3554.
(7) Thorson, M. R.; Goyal, S.; Schudel, B. R.; Zukoski, C. F.; Zhang, G. G.; Gong, Y.; Kenis, P. J. A microfluidic platform for pharmaceutical salt screening. *Lab Chip* **2011**, *11*, 3829−3837.
(8) Park, D. S.-W.; Wang, H.; Chen, P.-C.; Park, T.; Kim, N.; You, B.; Nikitopoulos, D.; Soper, S.; Murphy, M. Passive micro-assembly of a fluidic control chip and a multi-well continuous flow PCR chip for high throughput applications. In *Proceedings of 14th International Conference on Miniaturized Systems for Chemistry and Life Sciences*; Chemical and Biological Microsystems Society (CBMS), 2010; pp 1226−1228.
(9) Chen, P.-C.; Park, D. S.; You, B.-H.; Kim, N.; Park, T.; Soper, S. A.; Nikitopoulos, D. E.; Murphy, M. C. Titer-plate formatted continuous flow thermal reactors: Design and performance of a nanoliter reactor. *Sens. Actuators, B* **2010**, *149*, 291−300.
(10) Brennan, M. D.; Rexius-Hall, M. L.; Eddington, D. T. A 3D-printed oxygen control insert for a 24-well plate. *PLoS One* **2015**, *10*, No. e0137631.
(11) Simone, E.; McVeigh, J.; Reis, N. M.; Nagy, Z. A high-throughput multi-microfluidic crystal generator (MMicroCryGen) platform for facile screening of polymorphism and crystal morphology for pharmaceutical compounds. *Lab Chip* **2018**, *18*, 2235−2245.
(12) Park, D. S.-W.; Chen, P.-C.; You, B. H.; Kim, N.; Park, T.; Lee, T. Y.; Datta, P.; Desta, Y.; Soper, S. A.; Nikitopoulos, D. E.; et al. Titer plate formatted continuous flow thermal reactors for high throughput applications: fabrication and testing. *J. Micromech. Microeng.* **2010**, *20*, 055003.
(13) Park, D.; Chen, P.-C.; You, B.; Kim, N.; Park, T.; Datta, P.; Desta, Y.; Soper, S.; Nikitopoulos, D.; Murphy, M. Optimization of Geometry for Continuous Flow PCR Devices in a Titer Plate-Based PCR Multi-Reactor Platform. *ASME International Mechanical Engineering Congress and Exposition*; ASME, 2007; Vol. *4305*, pp 113−118.
(14) Lai, B. F. L.; Lu, R. X. Z.; Davenport Huyer, L.; Kakinoki, S.; Yazbeck, J.; Wang, E. Y.; Wu, Q.; Zhang, B.; Radisic, M. A well plate-based multiplexed platform for incorporation of organoids into an organ-on-a-chip system with a perfusable vasculature. *Nat. Protoc.* **2021**, *16*, 2158−2189.
(15) Coliaie, P.; Kelkar, M. S.; Nere, N. K.; Singh, M. R. Continuous-flow, well-mixed, microfluidic crystallization device for screening of polymorphs, morphology, and crystallization kinetics at controlled supersaturation. *Lab Chip* **2019**, *19*, 2373−2382.
(16) Coliaie, P.; Kelkar, M. S.; Langston, M.; Liu, C.; Nazemifard, N.; Patience, D.; Skliar, D.; Nere, N. K.; Singh, M. R. Advanced Continuous-Flow Microfluidic Device for Parallel Screening of Crystal Polymorphs, Morphology and Kinetics at Controlled Supersaturation. *Lab Chip* **2021**, *21*, 2333−2342.
(17) Ding, X.; Mu, Y. Digital Nucleic Acid Detection Based on Microfluidic Lab-on-a-Chip Devices. *Lab-on-a-Chip Fabrication and Application*; IntechOpen, 2016; p 125.
(18) Xie, S.; Wu, J.; Tang, B.; Zhou, G.; Jin, M.; Shui, L. Large-area and high-throughput PDMS microfluidic chip fabrication assisted by vacuum airbag laminator. *Micromachines* **2017**, *8*, 218.
(19) Sweet, E.; Yang, B.; Chen, J.; Vickerman, R.; Lin, Y.; Long, A.; Jacobs, E.; Wu, T.; Mercier, C.; Jew, R.; et al. 3D microfluidic gradient generator for combination antimicrobial susceptibility testing. *Microsyst. Nanoeng.* **2020**, *6*, 92.
(20) Dertinger, S. K.; Chiu, D. T.; Jeon, N. L.; Whitesides, G. M. Generation of gradients having complex shapes using microfluidic networks. *Anal. Chem.* **2001**, *73*, 1240−1246.
(21) Davydova, E.; Wouters, S.; Deridder, S.; Desmet, G.; Eeltink, S.; Schoenmakers, P. J. Design and evaluation of microfluidic devices for two-dimensional spatial separations. *J. Chromatogr. A* **2016**, *1434*, 127−135.
(22) Karbalaei, A.; Cho, H. J. Microfluidic devices developed for and inspired by thermotaxis and chemotaxis. *Micromachines* **2018**, *9*, 149.
(23) Cachet, C.; Ganne, F.; Maurin, G.; Petitjean, J.; Vivier, V.; Wiart, R. EIS investigation of zinc dissolution in aerated sulfate medium. Part I: bulk zinc. *Electrochim. Acta* **2001**, *47*, 509−518.
(24) Kim, Y.-s.; Rousseau, R. W. Characterization and solid-state transformations of the pseudopolymorphic forms of sodium naproxen. *Cryst. Growth Des.* **2004**, *4*, 1211−1216.

https://doi.org/10.1021/acsomega.3c05478
ACS Omega 2023, 8, 41502−41511